ELSEVIER

Journal of Nuclear Materials 246 (1997) 232–243

journal of nuclear materials

On Raman spectroscopy of zirconium oxide films

P. Barberis [a,*], T. Merle-Méjean [b], P. Quintard [b]

[a] CEZUS Centre de Recherches, Avenue Paul Girod, 73403 Ugine, France

[b] Laboratoire de Matériaux Céramiques (LMCTS-URA 320), Faculté des Sciences, 123 Avenue Albert Thomas, 87060 Limoges, France

Received 21 March 1996; accepted 26 March 1997

Abstract

Using Raman spectroscopy, we studied samples of pure tetragonal and monoclinic zirconia powders, and oxide film developed at 400°C in steam (autoclave) on Zircaloy-4 with various tin contents. We analyze the absolute intensities of the bands and background, as well as the position of the bands. All these parameters bring some surprising evolution with tin content and oxidation time, relatively to the powders. We have shown that the films are mainly monoclinic, but that the second phase is not similar to the tetragonal phase observed in powders. It is probably a distorted tetragonal phase. The oxide films are not homogeneous through their thickness, being better crystallized near the surface. This prevents to compute directly any relevant tetragonal fraction from the band intensities. The presence of tin induces a high background, probably related to the existence of numerous oxygen vacancies. The absorption coefficient of the films at 514 nm is about 0.4 μm^{-1}.

1. Introduction

The corrosion mechanism of zirconium alloys is still unclear, despite numerous works published since more than thirty years. Although the classic observation methods like X-ray diffraction, electron microscopy and impedance spectroscopy are still very useful, some other techniques like photo electrochemistry, infrared spectroscopy and Raman spectroscopy have been used. In particular, Raman spectroscopy has been applied since the mid-seventies to the engineering ceramics. In a first approach, the different allotropic forms of zirconia have been characterized [1–5], after what the pressure–temperature diagram of this material has been investigated [6–8].

Some authors used the intensity ratios of different peaks to determine quantitatively the proportion of a phase in a mixture [9–13]. However, all these formula are empirical, because of the lack of data concerning the polarizability of each bond in the crystalline lattice, and its variation with the atoms vibrations. Still at atmospheric pressure, some studies investigated the effect of the oxide grain size on the peak width [14], and of the stabilizing additions of various oxides (like Nb_2O_5, Y_2O_3, CaO...) on the peak positions [15]. For, as for X-ray diffraction, a lot of parameters may affect the intensity, the position or the width of the Raman peaks as displayed in Table 1.

Some other studies investigated the pressure effect, and the high pressure phases. It has been evidenced that the peak positions of monoclinic zirconia shift when increasing the pressure, and that at room temperature, a new phase appears at about, 5 GPa [6]. After some controversy, this phase has been indexed in the orthorhombic system [16]. It is interesting to note that this phase, due to a lattice cell double to the tetragonal one, presents a relatively low degree of symmetry, and thus a lot of Raman peaks [8].

On another hand, zirconium specialists applied Raman spectroscopy to the study of oxide films developed either during high temperature autoclave exposures in steam or water, or in nuclear reactor.

Godlewski et al. [17,18] performed Raman investigations on Zy-4 oxide films formed in autoclave at 400°C.

* Corresponding author. Tel.: +33-4 79 89 30 30; fax: +33-4 79 89 35 00.

0022-3115/97/$17.00
PII S0022-3115(97)00038-X

Table 1
Parameters affecting the Raman bands

Parameters	Band position	Band intensity	Band width
Crystal size	×		×
Stresses	×	×	×
Stoichiometry	×	×	
Alloying elements	×	×	×
Texture (preferential orientation)	–	×	–
Gradients of the previous parameters	×	×	×

They induced from their observations that the oxide was mainly monoclinic, the minor phase being tetragonal. On tapered sections, and assuming the relation obtained on powders by [9] was applicable, they determined the gradient of the tetragonal phase through the oxide thickness. They found three zones: near the metal/oxide interface a very thin layer (about 100 nm) with very high concentration of tetragonal phase (about 40%), then a plateau with about 15% of tetragonal phase, finally near the oxide surface, a very low level.

Doyle and Alvarez [19] investigated zirconia debris found in the primary circuit of the Three Miles Island nuclear power plant, and deduced their origin from their Raman spectra: they attributed tetragonal zirconia to zircaloy oxide films, stabilized by a crystallize size effect, and possibly by stresses or hydrogen. However, the peak-shifts origin was not fully understood, neither the 'non-standard' monoclinic spectra.

Finally, Cox [20] studied some oxide formed on different zirconium alloys in water with, in some cases, additions of lithium. He had some difficulties to obtain good Raman spectra on thin films. On thick films (5 μm) formed in steam, he found tetragonal zirconia at the surface of the sample, contrarily to what is observed in Refs. [17,18]. Only monoclinic phase was found on a sample corroded in lithiated water.

However none of these authors studied in details the recorded Raman spectra, and only a rough comparison with spectra obtained on zirconia powder (and often with chemically stabilized tetragonal zirconia powders) has been made.

In this paper, we acquired the Raman reference spectra of pure nanocrystallized tetragonal and monoclinic zirconia powders. We corroded in autoclave (steam at 400°C, 10.5 MPa) for 20 to 100 days two Zircaloy-4 type materials differing by their tin content. We recorded the Raman spectra of the oxide films and determined the absorption coefficient. Finally, by computer simulation we investigated the effect of stresses on the peak positions of the tetragonal phase.

2. Experiments

2.1. Materials

Zirconia powders were prepared by CRICERAM (now CEZUS Chimie) by reacting zirconium tetrachloride with steam at high temperature. The obtained powder is mainly tetragonal, with a grain size (as determined by X-ray diffraction) of about 15 nm. To obtain a monoclinic powder, the tetragonal powder was submitted to annealing at 900°C under O_2/H_2O mixture. Grain size was then about 30 nm. The chemical analysis is given in Table 2 together with the content of tetragonal phase. More detailed information about these powders can be found in Ref. [21].

Zircaloy materials are from the same sheets as the samples described in Ref. [22]. It is 'Zircaloy 4' with 1.2 or 0% Sn, in the form of 1 mm thick recrystallized sheets, produced at a laboratory scale by CEZUS. The chemical composition is given in Table 3. The oxidation was performed in a static autoclave, in steam at 400°C, for up to 100 days. The exact oxidation time and obtained weight gains for each sample are given in Table 4. Note that for the Zircaloy-4–1.2% Sn, there is a kinetic transition (deduced from the kinetic curve [22]) at about 40 days so that some samples are beyond the transition point. For Zircaloy-4–0% Sn, the transition occurs at 200 days and all the samples are before this point.

2.2. The Raman spectrometer

The Raman spectra were recorded using a Dilor spectrometer, X–Y model, in a back-scattering geometry. The spectra were excited from the 514.5 nm wavelength of an Ar^+-laser. A typical spectrum was obtained with a 50 mW laser power, during a total of 500 s, and a slit width set to 150 μm. The reproducibility in determining a peak position is better than 1 cm^{-1}. The area irradiated with the laser beam was either 700 μm^2 in the macroscopic mode or 1 μm^2 under microscope (only for the tetragonal powder).

Table 2
Chemical analysis of zirconia powder

	Hf (wt ppm)	Cl (wt %)	BET specific area (m^2/g)	Tetragonal content (as received)
ZrO_2	450	1.9	15.1	85%

Table 3
Chemical analysis of zirconium alloys

Alloy	Sn (wt%)	Fe (wt%)	Cr (wt%)	O (wt–ppm)
Zy-4–1.2% Sn	1.2	0.22	0.11	1300
Zy-4–0% Sn	0.0	0.20	0.11	900

Table 4
Characteristics of zircaloy samples and of Raman spectra recorded on these samples. The oxide films thickness has been deduced from the weight gains, assuming 1 μm of oxide equals 15 mg/dm^2. The tetragonal content have been computed from Raman spectra according to the formula given in Ref. [9]. The values obtained by X-ray diffraction have been taken in Ref. [22]

Alloy	Corrosion test (steam, 400°C)			Raman spectra		Tetragonal content (%)	
	oxidation time (days)	weight gain (mg/dm^2)	thickness (μm)	absolute intensity of the 478 cm^{-1} band (a.u.)	background at 478 cm^{-1} (a.u.)	Raman	XRD [22]
Zy-4–0% Sn	20	20	1.3	4300	700	27	6
Zy-4–0% Sn	100	35	2.3	6500	1000	17	7
Zy-4–1.2% Sn	20	25	1.7	2700	2800	22	8
Zy-4–1.2% Sn	40	32	2.1	3800	2900	16	8
Zy-4–1.2% Sn	60	44	2.9	4000	2500	10	7
Zy-4–1.2% Sn	80	52	3.4	4500	3200	8	6
Zy-4–1.2% Sn	100	57	3.8	7100	4000	7	6

2.3. Software

Two software have been used during this study. The first one, RXAJUST, developed by one of the authors (Barberis) allows the fitting of each peak by a Gaussian. The Raman bands of solids are usually fitted by Lorentzian/Gaussian mixtures. Fitting by Gaussians underestimates slightly the maximum intensity of the peaks, as can be seen in Fig. 1. If the bands are asymmetric, both methods can induce some bias in the band position.

The second one, CRYME (Crystal Mechanics) [23] allows to simulate vibrational (IR and Raman) spectra of a material, from a phenomenological model of inter-atomic potential functions. It can calculate at the same time macroscopic known characteristics such as elastic modulus, piezoelectric or dielectric constants or thermodynamical properties for a stress-free lattice or for a material under hydrostatic compression.

3. Results

3.1. Zirconia powders

The as received zirconia powder was mainly tetragonal. It has been annealed for 24 h at 900°C in a O_2/H_2O mixture to obtain a fully monoclinic powder. The spectra recorded on the two powders (as received and annealed) are presented in Figs. 1 and 2, while the band parameters are listed in Tables 5 and 6.

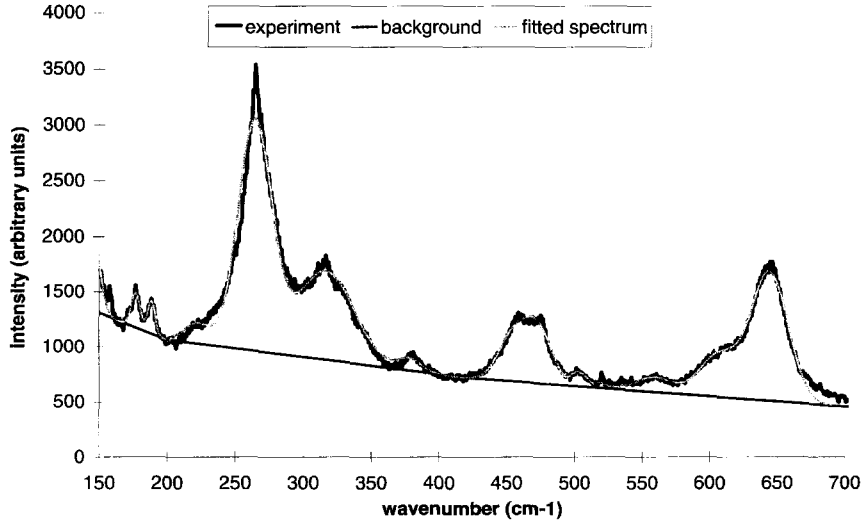

Fig. 1. Experimental and fitted micro-Raman spectrum of a nanocrystalline tetragonal zirconia powder (the analyzed area was about 1 μm^2).

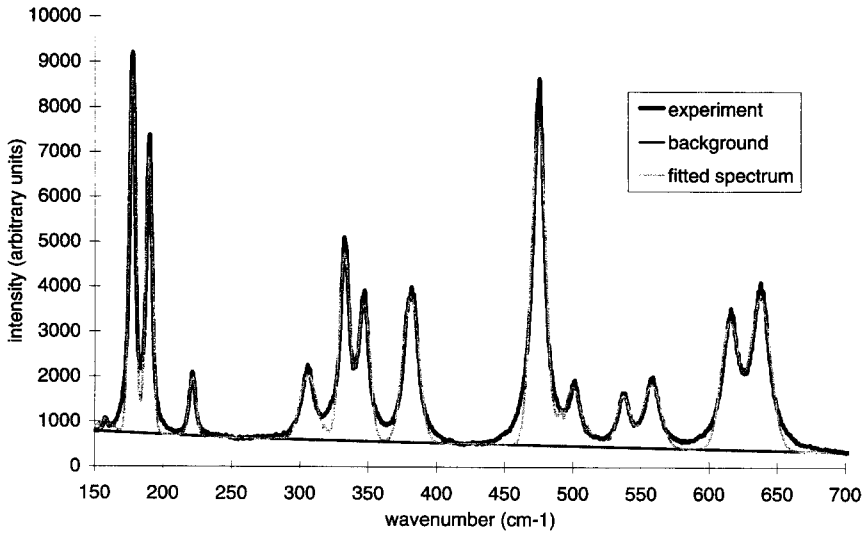

Fig. 2. Experimental and fitted macro-Raman spectrum of a pure nanocrystalline monoclinic zirconia powder (the analyzed area was about 700 μm^2).

The monoclinic powder presents very well defined peaks, the more intense of which are located at 475, 177 and 190 cm^{-1}. The as-received powder exhibits much broader bands, the more intense being at 266 and 644 cm^{-1}. The three above mentioned peaks of the monoclinic phase are visible, indicating that monoclinic phase is present in the as-received sample. This is in agreement with the X-ray diffraction data.

Table 5
Band positions, intensities (relative to the more intense 267 cm^{-1} band) and width of the as-received mainly tetragonal zirconia. Several bands assigned to the monoclinic phase are present, but weak

Peak position (cm^{-1})	Relative intensity (%)	Peak width (cm^{-1})	Attribution
145.9	12.8	11.7	T
176.8	3.5	7.9	M
188.4	2.9	7.0	M
223.5	8.6	30.4	M
267.1	*100.0*	*33.6*	*T*
315.1	42.6	33.6	T
332.4	2.4	9.7	M
344.9	6.5	18.7	M
380.5	3.8	17.6	M
456	18.2	28.0	T
473.7	13.4	21.9	M
502.9	5.4	37.8	M
558.9	8.0	43.5	M
607.1	20.1	35.4	T
644.5	57.3	34.0	T

3.2. Absorption coefficient of the oxide film

To determine the absorption coefficient of the oxide films at 514.5 mn (laser wavelength), we removed the metal from the oxide film on a part of the corrosion sample by chemical etching in a classical $HF/HNO_3/H_2O$ bath. We obtained portions of oxide of several tens of μm in diameter, without the metallic matrix. Then we put the sample under a microscope illuminated by the laser light, and measured the transmitted beam intensity I with a

Table 6
Band positions, intensities (relative to the more intense 475 cm^{-1} band) and width of the heat treated monoclinic zirconia

Peak position (cm^{-1})	Relative intensity (%)	Width (cm^{-1})	Attribution
158.0	1.3	4.1	M
177.4	52.4	6.1	M
189.5	42.6	6.4	M
221.4	9.3	6.5	M
306.0	23.2	14.8	M
332.5	42.8	9.5	M
346.6	37.1	11.1	M
381.1	51.4	14.6	M
474.6	100	12.7	M
500.2	20.4	14.4	M
537.1	14.9	12.1	M
557.9	25.4	16.6	M
615.2	49.6	16.2	M
637.6	69.0	18.9	M

Table 7
Characteristics of the samples and their absorption coefficient μ

Alloy	Oxidation time (days)	Oxide thickness (μm)	μ (μm^{-1}) (standard deviation)
Zy-4–1.2% Sn	100	4.7	0.42 (0.09)
Zy-4–0% Sn	120	2.3	0.37 (0.08)

photoelectric cell. The absorption coefficient μ was then computed according to the formula

$$I = I_0 \exp(-\mu t), \quad (1)$$

where I_0 is the incident beam intensity and t the film thickness determined by the weight gain (1 μm of oxide corresponds to 15 mg/dm^2, with an accuracy of 0.05 μm).

Two samples were measured in such a way. Their characteristics are displayed in Table 7 together with the mean value and standard deviation of the absorption coefficient (over 10 different measurements). It is assumed that the chemical etching does not alter the film, and that the thickness is constant over the film.

The μ values are about 0.4 μm^{-1} and are not significantly different, so that, on a few μm thick films, a significant part of the incident laser beam penetrates the oxide down to the metal/oxide interface, and can reflect there.

3.3. Zircaloy oxide films

Four to six spectra were recorded on each sample (Zy-4 with 0% or 1.2% Sn, oxidized from 20 to 100 days). Four of these are presented in Fig. 3, corresponding to some samples. It was checked that the oxide films undergo no observable transformation (no change on the Raman spectra) under the laser beam: it is thought that with our conditions, the local temperature measured from Stokes/Antistokes Raman intensities does not exceed 150°C, during a few minutes. Thus, recording repeatedly spectra without moving the sample does not induce any change on the spectra. On the contrary, we observed some changes if the laser power is increased to 400 mW.

For each spectrum, the peaks positions, intensities (relative to the more intense monoclinic peak at about 474 cm^{-1}), integral widths and shifts (the shift is defined here as the difference between the actual peak position and the position of the equivalent peak recorded on powders) were computed. Their mean values (over 4–6 spectra) are presented in Table 8 and in Fig. 4. The absolute intensity (above the background), and the background at 475 cm^{-1} are given in Table 4.

We can draw readily the following observations.

(i) Concerning the general form of the spectra, the main influence of the tin content is seen on the signal/background ratio. This ratio is higher for the lower tin content. For that reason, the peak parameters (position, intensity, width) will be more accurate for the low tin content.

(ii) The most important point is that the bands at about 280, 444 and 235 cm^{-1} are not found on powders and become weaker when increasing the oxidation time, and disappear on the Zy-4–1.2% Sn after 100 days of corrosion.

(iii) For all the other bands, the parameters are not very dependent on the tin content and oxidation time (Table 8) and the small differences which appear are within the experimental errors. However, we observe a small shift between the position of a monoclinic peak in the powder

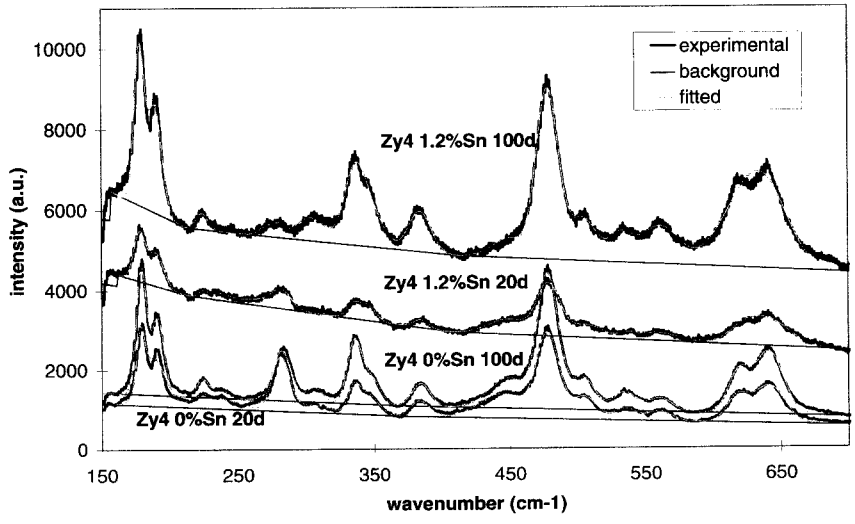

Fig. 3. Experimental and fitted macro-Raman spectra of four oxide films, recorded in exactly the same experimental conditions, so that the absolute intensities should be comparable. The analyzed area was about 700 μm^2. Note the higher background on the high tin-content samples.

Table 8
Band positions, intensities (relative to the more intense 475 cm^{-1} band), width and shift of the bands observed on the four oxidized zircaloy samples. The shifts are computed by subtracting the band position on the sample from the band position on the powder. Concerning the band at about 280 and 444 cm^{-1} on the samples, the references on the powder have been taken as 267 and 458 cm^{-1}

Zy-4–1.2% Sn, 20 days				Zy-4–1.2% Sn, 100 days				Zy-4–0% Sn, 20 days				Zy-4–0% Sn, 100 days			
position (cm^{-1})	relative intensity (cm^{-1})	width (cm^{-1})	shift (cm^{-1})	position (cm^{-1})	relative intensity (cm^{-1})	width (cm^{-1})	shift (cm^{-1})	position (cm^{-1})	relative intensity (cm^{-1})	width (cm^{-1})	shift (cm^{-1})	position (cm^{-1})	relative intensity (cm^{-1})	width (cm^{-1})	shift (cm^{-1})
158.1	4.7	22.5	−0.6	158.2	9.8	18.0	−0.6	159.6	5.9	16.3	−2.1	159.7	8.4	20.8	−2.2
175.5	35.2	9.6	1.9	175.9	43.8	9.6	1.6	176.7	36.5	10.1	0.7	176.7	40.6	8.8	0.7
186.4	41.7	14.8	3.2	187.0	40.2	12.9	2.5	188.0	42.9	14.9	1.5	187.7	46.7	14.8	1.8
221.4	6.2	17.2	0.0	220.6	8.2	20.7	0.8	221.2	12.1	24.8	0.2	221.3	7.7	11.2	0.1
235.6	2.1	24.3						236.7	6.2	24.2		235.1	3.7	15.3	
281.7	21.1	18.6	−14.7	280.7	6.2	17.8	−13.7	282.2	28.7	16.4	−15.2	282.8	17.4	12.3	−15.8
305.6	13.8	29.5	0.7	304.1	11.8	23.6	2.2	305.2	10.0	20.2	1.1	305.4	10.0	26.2	1.0
334.1	30.6	18.1	−1.6	333.2	38.7	18.9	−0.7	332.6	28.2	18.5	−0.1	334.0	28.2	13.3	−1.5
343.9	20.2	19.6	2.7	344.8	20.7	22.6	1.8	343.7	14.8	21.8	19.3	346.2	14.8	14.6	0.4
381.4	15.0	18.2	−0.2	381.1	21.5	21.3	0.0	383.5	12.6	21.5	−2.4	382.2	13.0	15.5	−1.0
443.4	31.0	29.4	14.6	450.1 [a]	18.8 [a]	30.0 [a]	12.9 [a]	443.2	48.9	32.8	14.8	443.7	28.8	29.3	14.3
476.0	100.0	24.9	−1.4	475.7	100.0	26.0	−1.0	475.2	100.0	24.7	−0.6	476.2	100.0	21.5	−1.6
503.4	23.8	22.0	−3.0	502.8	29.9	26.8	−2.4	501.9	19.3	18.4	−1.5	502.0	18.9	17.9	−1.6
				534.4	8.3	20.8	2.9	532.9	13.2	21.5	4.4	533.3	11.4	21.5	4.0
561.2	24.7	29.5	−3.0	560.4	35.5	41.9	−2.2	558.5	14.7	25.9	−0.3	559.3	9.7	20.7	−1.1
621.3	32.4	35.6	−6.0	618.2	21.9	35.5	−2.9	616.5	28.2	34.9	−1.2	614.7	22.6	19.8	0.6
639.7	102.5	47.1	−1.9	635.6	109.3	57.7	2.2	637.5	74.7	42.9	0.2	638.0	59.1	30.8	−0.3

[a] With lower accuracy: this band is a weak shoulder on the intense 476 cm^{-1} band.

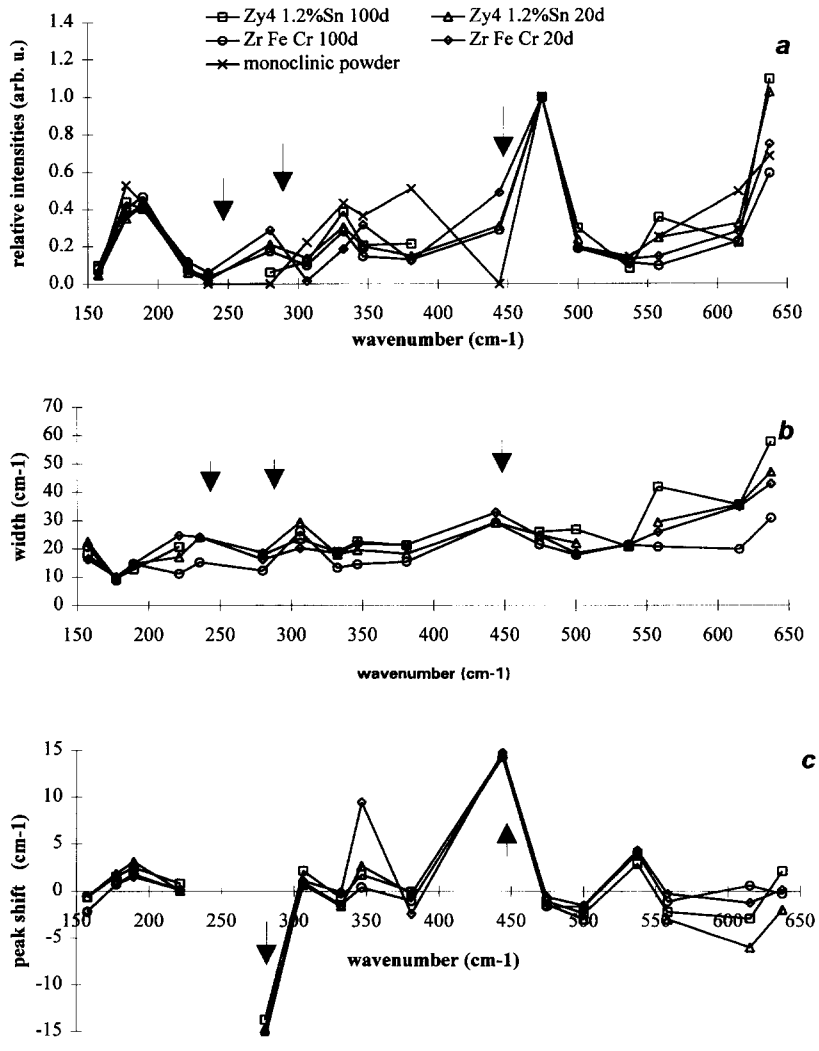

Fig. 4. Comparison of the bands relative intensities (a), widths (b) and positions (c) between the four oxide films samples and the monoclinic powder. The arrows indicate non-monoclinic features.

and in the film (see Table 8 and Fig. 4c). This shift can be positive or negative, depending on the considered peak and could be attributed to the stresses or the non-stoichiometry of the oxide films.

3.4. Computation of the effect of isotropic stresses

The infrared and Raman spectra of the tetragonal crystal were computed from CRYME software using a simple valence force field. The interatomic potential was built from a few force constants. First, two stretching force constants described the two kinds of Zr–O bonds, K_1 for the Zr–O short bonds (2.1 Å) and K_2 for the Zr–O long bonds (2.4 Å). The initial values were determined from previous works [5,24] (Fig. 5): $K_1 = 1.5$ N cm^{-1} and $K_2 = 0.8$ N cm^{-1}. Secondly, the third force constant K_3 representing the O–O interactions in the edges of the ZrO_8 polyhedron was evaluated from the data given by Iishi [25]: $K_3 = 0.75$ N cm^{-1}. Then, two off-diagonal force constants were added, showing the interactions between two adjacent Zr–O bonds, the O–Zr–O angles of which were respectively equal to 70.5 and 109.5°: $H_1 = 0.14$ N cm^{-1} and $H_2 = -0.14$ N cm^{-1}. The K and H values were adjusted by fitting procedure to reproduce the IR and Raman spectra with the Cij lattice constants of the tetragonal crystal [26].

Moreover, the knowledge of the C_{ij} constants allows to compute the changes in the bond length and angles under external isotropic pressure: we found a variation of 0.0045 Å GPa^{-1} and 0.0018 Å GPa^{-1} for the short and long Zr–O bonds respectively. From these data and using the 'interatomic force constant-interaction bond length' depen-

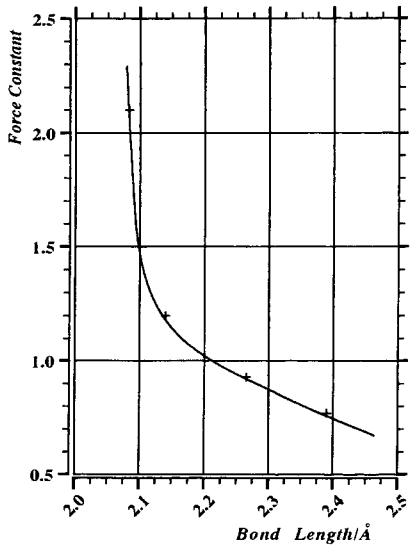

Fig. 5. Force constant of Zr–O stretching (N cm^{-1}) versus bond length.

dence, we obtained the new magnitudes of the K_1, K_2 and K_3 forces for given pressure, then we calculated the relevant spectra and deduced the frequency changes $\Delta\varpi$. The frequency shifts of the characteristic tetragonal Raman active bands were respectively 0.7 and 1 cm^{-1} GPa^{-1} for the 145 and 266 cm^{-1} bands. According to X-ray diffraction experiments, the stresses in the oxide layers were estimated to be from 1 to 3 Gpa, which would lead to a frequency shift less than 3 cm^{-1}.

4. Discussion

4.1. Analyzed thickness of the oxide film

The value of the absorption coefficient we determined indicates that the signal will come mainly from the first few microns of the film, and not only from the 50 nm at the extreme surface. It can thus explain why Cox [20] could not obtain a good signal/noise ratio on thin (0.6 μm) films.

Another consequence is that the laser beam may reflect at the metal oxide interface when a nearly parallel beam is used as in macro-Raman. We can compute what is the collected intensity as a function of the oxide thickness with and without this reflection. The computation is straightforward:

$$I(t) = \alpha I_0 \int_0^t \exp(-2\mu x)\mathrm{d}x + \alpha I_0 \exp(-\mu t) \int_0^t \exp(-(t-x))\exp(-x)\mathrm{d}x, \quad (2)$$

that is

$$I(t) = \alpha I_0 \left\{ \frac{1-\exp(-2\mu t)}{2\mu} + t\exp(-2\mu t) \right\}, \quad (3)$$

where $I(t)$ is the collected intensity for a given film thickness t, x is the depth in the film (and equals 0 at the surface, t at the metal/oxide interface) and α represents the scattered part of the radiation.

The first term gives the intensity that would be collected without reflection at the interface (as for example in micro-Raman), the second term the part due to the reflection. For these computations, we assumed the interface to be exactly perpendicular to the laser beam, without any roughness. It is of course not the case for the actual oxide films, so that the above formula will give only the maximum intensity that could be observed with reflection.

The function $I(t)$ is plotted in Fig. 6 for $\mu = 0.4$ μm^{-1} both with and without reflection. We can see that without reflection, we have the classical monotonous curve with an asymptote: very few information comes from a depth greater than 4 μm. At the contrary, when we take the reflection into account, the curve is no longer monotonous, but shows a maximum at about 2 μm. In addition, for the thinner films, the intensity is much greater than it would be without reflection. An interesting fact is that for oxide film thicknesses greater than about 1 μm, the collected intensity is not expected to vary from more than ±10% from the asymptotic value. It is thus almost impossible to correlate the film thickness and the Raman peak intensity.

4.2. Peak positions

4.2.1. Powders

The peak positions determined for the powders are in very good agreement with literature values [1–4]. The discrepancies reach only 2–3 cm^{-1} for the strongest peaks on the monoclinic phase. For the tetragonal phase, the discrepancies raise up to 8 cm^{-1}. Two assumptions can be made. First, the literature data are often obtained on partially stabilized powders, and can thus be shifted. Secondly, the peaks are broad and often asymmetric.

In the following sections, we take our powder spectra as standards, and scale all the observations to them.

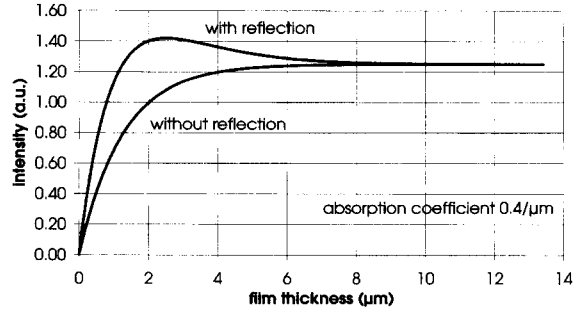

Fig. 6. Theoretical variation of the recorded intensity when varying only the film thickness. Two cases have been considered: the case where the oxide/metal interface reflects perfectly the incident beam, and the case where the reflection does not occur.

4.2.2. Comparison of zirconia powders and zircaloy oxide films spectra

Comparing powder and film spectra (Tables 5–7), we identify clearly on the films a first set of peaks that can be assigned to the monoclinic phase. In fact, all the bands observed on the monoclinic powder are present in the films spectra, although with sometimes weaker relative intensities. The peak shifts (as defined in Section 3 and as presented in Fig. 4c) are not exceeding 5 cm^{-1}, and only 3 cm^{-1} for the more intense. According to the measurement accuracy, only a few bands exhibit a relative intensity different from the powder. The more pronounced effect is observed on the 380 cm^{-1} band. This difference could be attributed to the strong texture (preferential orientation) of the oxide film.

A second set includes the 280, 444 and 235 cm^{-1} peaks. The first one has been assigned to the tetragonal phase [18] (and indexed at about 274 cm^{-1}). The others have not yet been evidenced, being often only a shoulder of the more intense monoclinic 475 or 221 cm^{-1} peaks. The intensity ratio $I(444)/I(280)$ and $I(235)/I(280)$ are almost independent on the sample, and about 1.5 and 0.2 respectively. This very important feature indicates that these peaks belong to the same phase.

Two hypotheses can be raised:

(i) they belong to the tetragonal phase and are shifted either by chemical alloying, compressive stresses, or non-stoichiometry;

(ii) they belong to the orthorhombic (high pressure) phase.

This second hypothesis would nicely explain the presence of the 444 and 235 cm^{-1} peak, since published data exhibit bands at about 441 and 228 cm^{-1} when 'quenched' at room pressure [8]. However this phase exhibits no peak at about 280 cm^{-1}, the nearest being at 228 and 313 cm^{-1}. In addition we observe no other band that can be assigned to this phase, although the 202, 359 and 405 cm^{-1} peaks are more intense than the 441 cm^{-1} peak on powders.

Assigning these peaks to the tetragonal phase does not solve all the problems. It would mean that the 267 and 456 cm^{-1} are shifted of about +13 and −12 cm^{-1} respectively. No peak is visible near 235 cm^{-1} in the tetragonal powder. In addition, the intensity ratio of these bands is very different on powder and films: $I(456)/I(267)$ is about 0.2 on powder, and about 1.5 on films.

These peaks are observed, although with varying intensities (relative to the more intense monoclinic band), on both 'zircaloys' oxide films. Their position is not affected by the tin content. The other addition elements (Fe, Cr), are essentially precipitated in the metal (only a minor fraction, let us say 100 ppm, is in solid solution). In the oxide films, it is known that the second phase particles oxidize and that the iron can dissolve in the surrounding oxide [27]. However, the oxide films investigated in this study are thin and the iron is likely not to be rejected from the second phase particles. So, the chemical shift seems to be excluded.

Another possible explanation is a shift due to stresses. We have demonstrated in Section 3.4 that, for an isotropic pressure, the shift of the most characteristic tetragonal band (264 cm^{-1}) would be of about 1.0 cm^{-1} GPa^{-1}. This would imply compressive stresses of about 15 GPa, that is far greater than the (mean) measured values [28,29]. In addition, it is likely that stresses would affect also the monoclinic peaks in a comparable manner, which is not observed. It can thus be concluded that isotropic (and likely non-isotropic) stresses are not relevant in this problem.

We assume that these bands should be attributed to a distorted tetragonal phase, with atom positions in the cell and lattice spacings slightly different from what is known on powders. It should be very difficult to ascertain this point by X-ray diffraction studies, since the 'tetragonal' phase exhibits only one peak distinct from the monoclinic phase which is the main phase in the oxide layer. This distortion could be induced by non-stoichiometry (the non-stoichiometry is one of the parameters that could stabilize the tetragonal phase). This would be coherent with the assumed increase of the non-stoichiometry near the metal–oxide interface, in correlation with higher tetragonal content. Yet, the difficulty is to consider that only the tetragonal phase is non-stoichiometric, since monoclinic bands are not shifted.

It is worth noting also that the monoclinic peak widths are much smaller on the powder than on the films. This fact cannot be attributed to the grain size, since the monoclinic powder exhibits a crystallite size of about 30 nm (determined by X-ray diffraction), comparable to the diameter of the columns in the oxide films. It could be due to some higher 'disorder' (non-stoichiometry, stresses, ...) in the films than in the powder.

4.3. Evolution of the film spectra with the tin content and the oxidation time

4.3.1. Absolute intensities of signal and background

In Fig. 3 are drawn four spectra in arbitrary but comparable units for the intensities: as they have been recorded with exactly the same parameters (laser power, counting time, ...), we can compare directly the intensities. For clarity we will speak of the intensities of the band at 480 cm^{-1} (which is the more intense monoclinic band) and of the background just at the same wave number (it is high enough to avoid a possible contribution from the Rayleigh band). These numbers are given in Table 4. But the conclusions hold at least qualitatively for the whole spectra.

4.3.1.1. Influence of the tin content. As mentioned previously, the spectra recorded on the films developed on Zy-4–1.2% Sn exhibit a much higher background than for

Zy-4–0% Sn. The background has several origins among which in our case: the reflected beam; the possible 'fluorescence' of some addition elements; the existence in the oxide layers of electronic defects.

The first one is due either to the high refractive index of zirconia ($n \sim 2$) which induces about 15% of the incident beam to be reflected at the oxide surface or to the thinness of the films which allows an unnegligible part of the beam to be reflected at the metal/oxide interface, thus increasing the spectra background for low wavenumbers, due to Rayleigh scattering. It could depend on the metal/oxide interface roughness, and thus on the alloy composition and oxidation time. It can be at least partly eliminated by tilting the sample when recording the spectra. For instance are given in Fig. 7 three spectra obtained on the same sample with an incident beam perpendicular to the oxide/metal interface or tilted of 5° and 15°. The background diminishes considerably with the tilt angle, so that the tilted position should be preferred.

The second hypothesis is the fluorescence of tin which is the only varying chemical parameter. Tin is assumed to be in solid solution in the metal matrix, and to be incorporated at the same time that zirconium: the tin atoms occupy substitutionnaly the cations sites in the oxide network. The fluorescence of the tin could explain the higher background on the Zy-4–1.2% Sn spectra. Another explanation is to assume that the presence of tin could induce a higher density of electronic defects in the layer. In the oxide layer, the tin should oxidize later than the zirconium (from a thermodynamical point of view, following the idea of Pêcheur et al. [27]). It would not be surprising to find tin atoms in oxidation states lower than four (the most stable) near the metal/oxide interface. Electrons would be trapped in the vacancies near these atoms, and thus perturb the Raman signal. Another experimental feature that could argue in favour of these two last explanations is that preliminary spectra recorded on oxidized Zr1%Nb samples are very similar to Zy-4–0% Sn spectra concerning the signal/background ratio. In this case, Nb is in solid solution to a significant amount (about 0.6%) in the metal phase, like Sn in Zy-4. Nb is thought to oxidize at the same time that the surrounding matrix, thus without creating any electronic defects.

4.3.1.2. Influence of the oxidation time. It is seen (Table 4) that

(a) the absolute intensity of the 476 cm^{-1} band increases much more with oxide thickness that what can be computed assuming the oxide layer homogeneous (Fig. 6),

(b) the signal/background ratio increases with oxidation time,

(c) the kinetic transition does not seem to induce a sharp modification. This can be interpreted by a gradient (of stresses, stoichiometry, crystallinity) through the oxide layer (the outer part being more relaxed, stoichiometric or better crystallized), and its evolution with the annealing time in autoclave.

4.3.2. Peak evolution

When the oxidation time and/or tin content are varied, we note two evolutions (Table 8):

(i) the relative intensities of the 280 and 444 cm^{-1} peaks decrease when increasing the oxidation time and/or the tin content;

(ii) the peak widths of the Zy-4–0% Sn 100 days are systematically smaller than for all other samples. This could be attributed to a better crystallization (larger grains and/or less point defects) in this oxide film as proposed by Barberis from X-ray diffraction experiments [22]. However, this should be confirmed by more precise work since it should be observed also on Zy-4–1.2% Sn when increasing the oxidation duration.

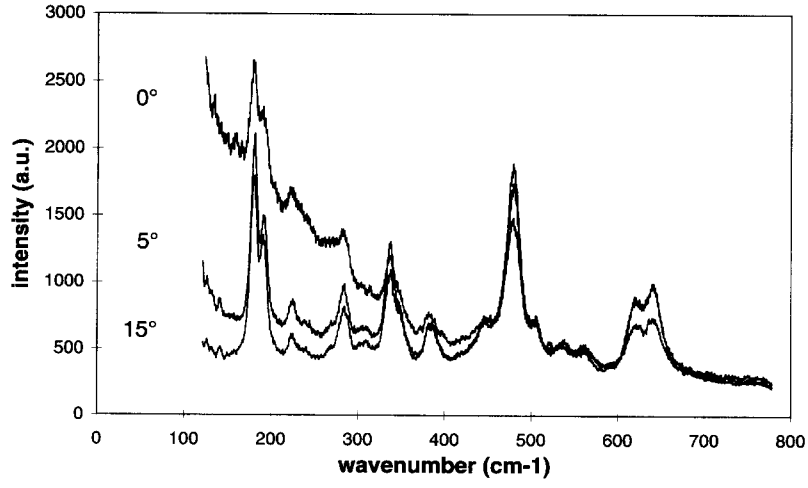

Fig. 7. Influence of the tilt angle on the Raman spectrum.

4.4. Tetragonal evolution in oxide films — comparison with X-ray diffraction data

As we mentioned previously, the relative intensities of 280 and 444 cm^{-1} peaks evolves with the tin content and the oxidation time. These peaks have been attributed to a distorted tetragonal phase. It would be interesting to compute the apparent proportion of this phase within the monoclinic oxide. This has been done by Godlewski and al. [18] using the following formula:

$$\%t = \frac{I(280)}{I(280) + I(179) + I(189)}, \quad (4)$$

where I represents the intensity of the corresponding peak.

This formula is likely biased: it has been established on stabilized tetragonal zirconia [9], with bands at 264 instead of 280 cm^{-1}. In addition, we have seen that the intensity depends on the tin content, the oxidation time and it is not evident that the evolution is the same for the tetragonal and monoclinic bands. So we think the proportions we can compute with this expression have, at this time, no meaning. We give the following values (Table 4), knowing the restrictions, to be able to compare with other works.

It is seen that the 'tetragonal content': decreases when increasing the corrosion time; decreases when increasing the tin content; is much higher than that determined by X-ray diffraction.

The first result is in agreement with several other works [17,18,22,28–30], but the evolution with tin content is in apparent contradiction with X-ray diffraction works [22,30]. One cause of this discrepancy could arise from the fact that the Raman is sensitive to local order while X-rays investigate the long range order. We could assume tetragonal-like structures of only a few nm in dimensions exists in the oxide, specially at the metal/oxide interface. We can notice that the tetragonal contents deduced from X-ray and Raman experiments 'converge' for large thicknesses.

5. Conclusion

We recorded Raman spectra on pure tetragonal and monoclinic zirconia powders, and on oxide films developed during 400°C autoclave corrosion on Zy-4 with 0% or 1.2% Sn.

We obtained the following results.

The absorption coefficient of the oxide films at 514 nm seems to be independent on the tin content, and is about 0.4 μm^{-1}.

All the peaks observed on the monoclinic powder are found on the oxide films, without any shift in the position, regardless of the tin content and oxidation time. However, the relative intensities of the peaks are slightly different on the films and on the powders, which could be attributed to the texture of the films. Three additional peaks (relative to the monoclinic powder spectrum) are observed at about 235, 280 and 444 cm^{-1} regardless of the tin content and oxidation time. They could be assigned to a distorted tetragonal phase, which structure is yet unknown, but not to the high pressure orthorhombic phase.

The absolute intensities of the Raman band do not vary as expected from the thickness of the oxide. It means that the oxide film is not homogeneous, and better crystallized in the outer region (far from the metal/oxide interface). Tin also affects the intensities. To give correct quantitative values of the tetragonal content in the oxide layer will thus need further work and knowledge of the impact of crystallization on Raman intensities.

The presence of tin in the oxide film induces a high background, possibly related to a high concentration of oxygen vacancies in the film near the metal/oxide interface where the tin atoms should not be totally oxidized.

Acknowledgements

We gratefully acknowledge Dr C. Lemaignan (CEA Grenoble, France) for helpful discussions on the oxide films microstructure and the role of addition elements. We thank Professor G. Lucazeau (ENSEEG, France) for comments on Raman spectroscopy and Dr A.P. Mirgorodsky (St. Petersburg, Russia) for help in simulations.

References

[1] C.M. Phillipi, K.S. Mazdiyasni, J. Am. Ceram. Soc. 54 (1971) 254.
[2] D.P.C. Thackeray, Spectrochim. Acta 30A (1974) 49.
[3] E. Anastassakis, B. Papanicolaou, I.M. Ashers, J. Phys. Chem. Solids 36 (1975) 667.
[4] M.A. Krebs, R.A. Condrate Sr., J. Am. Ceram. Soc. 67 (1982) C144.
[5] D. Michel, M.T. Van den Bone, A. Ennaciri, Advances in Ceramics, The American Ceramic Society, Vol. 24: Science and Technology of Zirconia 111 (1988) 555.
[6] H. Arashi, M. Ishigame, Phys. Status Solidi (a)71 (1982) 313.
[7] H. Arashi, Geophys. Monogr. 39 (1987) 335.
[8] G. Kourouklis, E. Liarokapis, J. Am. Ceram. Soc. 74 (1991) 520.
[9] D.R. Clarke, F. Adar, J. Am. Ceram. Soc. 65 (1982) 284.
[10] N. Iwainoto, N. Umesaki, Thin Solid Films 127 (1985) 129.
[11] C.S. Lim, T.R. Finlayson, F. Ninio, J.R. Griffiths, J. Am. Ceram. Soc. 75 (1992) 1570.
[12] C. Kontoyannis, M. Orkoula, J. Mater. Sci. 29 (1994) 5316.
[13] G. Kontoyannis, G. Carountzos, J. Am. Ceram. Soc. 77 (1994) 2191.
[14] K. Matsui, H. Suzuki, M. Ohgai, J. Am. Ceram. Soc. 78 (1995) 146.
[15] D.J. Kim, H.J. Jung, J. Am. Ceram. Soc. 76 (1993) 2106.
[16] J.M. Leger, P.E. Tomaszewski, A. Atouf, A.S. Pereira, Phys. Rev. B47 (1993) 14075.

[17] J. Godlewski, PhD thesis, Université Technologique de Compiègne, France (1991).
[18] J. Godlewski, J.P. Gros, M. Lambertin, J.F. Wadier, H. Weidinger, ASTM-STP 1132 (1991) 416.
[19] T.E. Doyle, J.L. Alvarez, in: Mater. Science Research Vol. 19: Advances in Materials Characterization 11 (Plenum, New York, 1985) p. 155.
[20] B. Cox, C. Wu, J. Nucl. Mater. 199 (1993) 272.
[21] S. Ben Othmane, PhD thesis, University of Limoges (1993).
[22] P. Barberis, J. Nucl. Mater. 226 (1995) 34.
[23] M.B. Smirnov, A.P. Mirgorodsky, P.E. Quintard, J. Molec. Struct. 348 (1995) 159.
[24] M.T. Van Den Borre, E. Husson, J.P. Chatry, D. Michel, J. Raman Spectrosc. 14 (1979) 341.
[25] K. Iishi, Phys. Chem. Miner. 4 (1979) 341.
[26] S.K. Chan et al., J. Am. Ceram. Soc. 74 (1991) 1742.
[27] D. Pêcheur, F. Lefebvre, A.T. Motta, C. Lemaignan, D. Charquet, ASTM-STP 1245 (1994) 687.
[28] F. Garzarolli, H. Seidel, R. Tricot, J.P. Gros, ASTM-STP 1132 (1991) 395.
[29] G. Wikmark, P. Rudling, B. Lehtinen, B. Hutchinson, A. Oscarsson, E. Ahlberg, presented at the ASTM 11th International Symposium on Zirconium in the Nuclear Industry, Garmisch–Partenkirchen (Germany), Sept. 11–14, 1995.
[30] H.J. Beie, A. Mitwalsky, F. Garzarolli, H. Ruhmann, H.J. Sell, ASTM-STP 1245 (1994) 615.